RJC

RASĀYAN *J. Chem.*
Vol. 10 | No. 2 |652 - 664 | April - June | 2017
ISSN: 0974-1496 | e-ISSN: 0976-0083 | CODEN: RJCABP
http://www.rasayanjournal.com
http://www.rasayanjournal.co.in

INFLUENCE OF CARBON NANOTUBE REINFORCED TiO_2-Al_2O_3 COATING MIXTURE ON AISI 1020 SURFACE PERFORMANCE

P.Vijayanand[1,*], Amitesh Kumar[2], K. R. Vijaya Kumar[3], Nazir Hussain[4], P.Kumaran[5] and S. Arungalai Vendan[6]

[1]Department of Mechanical Engineering, Ranchi University, Ranchi-834001, (Jharkhand) India
[2]Department of Foundry Technology, NIFFT, Ranchi-834003, (Jharkhand) India
[3]Department of Mechanical Engineering, Dr.M.G.R Educational and Research Institute, Chennai-600095, (Tamil Nadu) India
[4]Department of Mechanical Engineering, CIT, Ranchi-835103, (Jharkhand) India
[5]Department of Automobile Engineering, Saveetha University, Saveetha Nagar, Chennai-602105, (Tamil Nadu) India
[6]School of Electrical Engineering, VIT University, Vellore-632014, (Tamil Nadu) India
*E-mail: vijayme2004@rediffmail.com

ABSTRACT

Evolution and extensive research on nano technology has yielded several positive facets in the surface engineering which alters the mechanical properties and metallurgical behaviour of substrates as desired by designs specified for critical applications. In this work, plasma spray coating on mild steel using the nanocomposite material of Al_2O_3 with 13%TiO_2 & 1%CNT is carried out to examine the mechanical and metallographic behaviours. The Nano composite material is coated on AISI 1020 substrate using a plasma spray technique. ASTM C-633 standards are followed while performing destructive testing to examine the strength of the bonding. The Nano-structured coat layer exhibit greater resistance to crack growth, higher bonding strength and hardness. The higher strength and toughness obtained is attributed to the formation of net structures. Further, the samples are investigated by using X-ray diffraction technique and microscopic techniques. Al_2O_3 phase shows dominance. Metallographic studies revealed that coating on the substrate illustrates various regions, including the ceramic layer (Al_2O_3 or Al_2O_3–13 weight% TiO_2) and the matrix, that show little variance due to the coating. Negligible or insignificant amount of spalling or delamination is observed in the coatings. Nevertheless, there is negligible number of visible pinholes in the coatings. Response surface methodology is employed to examine the performance measures and parametric dependencies.

Keywords: Al_2O_3, TiO_2, Nano composites, Metallographic, Thermal Spray, Coatings

INTRODUCTION

There are several challenges faced by engineers while selecting specific materials for structural components in diversified industrial sectors viz., marine, aerospace, automobile, nuclear, oil exploration etc that operates in hostile ambience with varying temperatures, pressure, corrosion and gas flow. The surface properties vary at the components bulk and are expected to sustain the dynamic changes in the physical phenomenon.[1] Thermal spray coating is an economical and technically viable method employed for enhancing surface properties in engineering applications. This process typically comprises of a gun used to heat a material to its solidus state and subsequently pass a gas to accelerate the material to the target substrate to impart superior surface properties.[1] Figure-1 Illustrates thermal spray process.

Owing to the high hardness exhibited by Alumina (Al_2O_3) it finds several applications in tribological applications. Typically, Al_2O_3 is deposited on the substrate of the mechanical parts improves the surface functionality of engineering parts. [2-4]

http://dx.doi.org/10.7324/RJC.2017.1021707

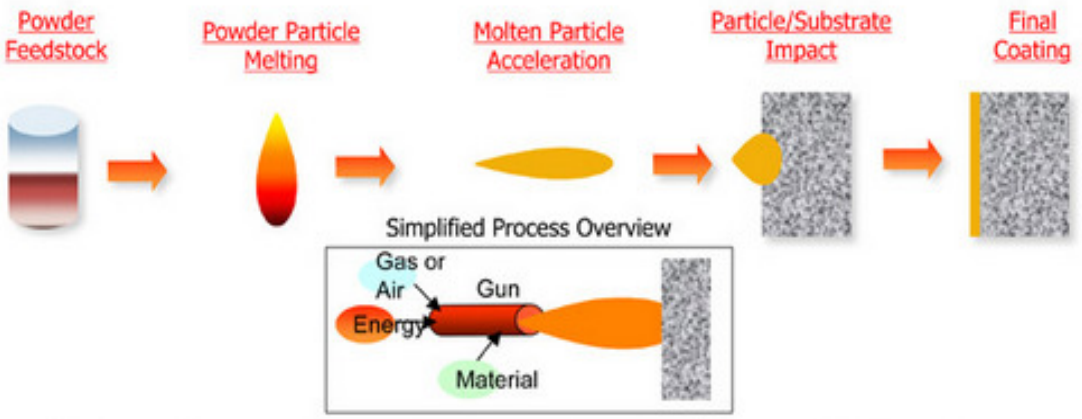

Fig.-1: Thermal Spray Technique[1]

Researchers have investigated and reported Al_2O_3-based nanocomposite coatings containing TiO_2.[5-8] The Al_2O_3/TiO_2 coatings exhibit greater wear resistance and higher toughness when compared to the elemental Al_2O_3 coatings alone.[9] Generally, plasma-sprayed Al_2O_3/TiO_2 coatings are created with commercial Al_2O_3-TiO_2 feedstock powders namely the METCO-130TM (Al_2O_3/13weight% (wt %) TiO_2).

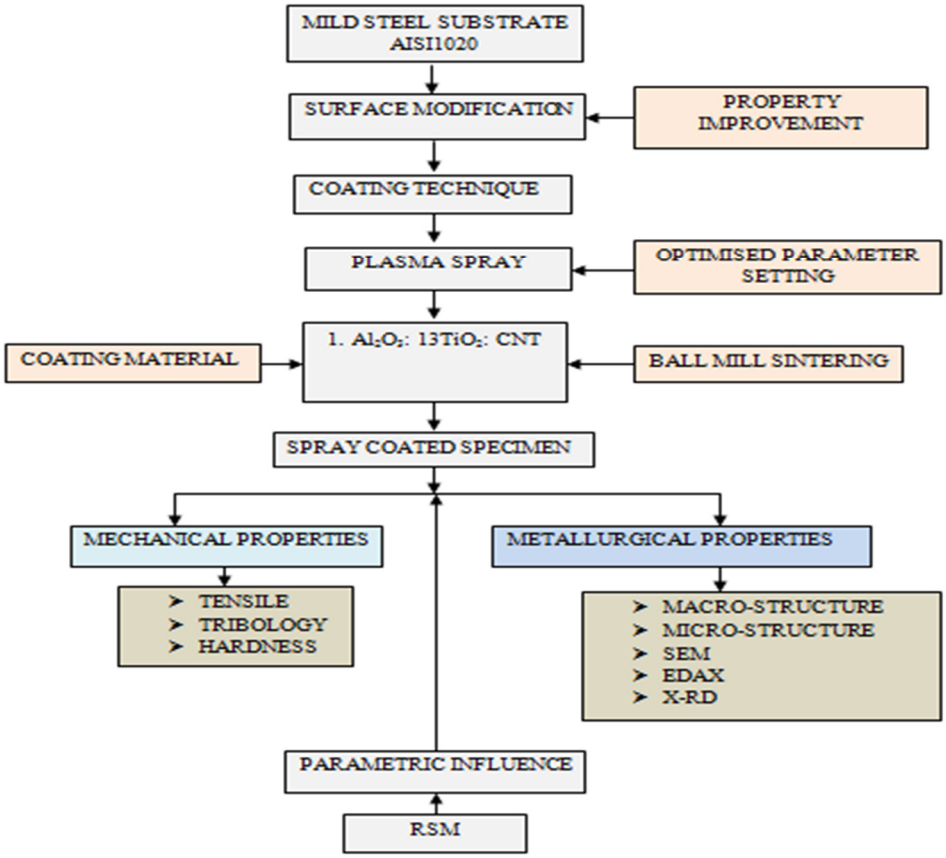

Fig.-2: Work Scheme for experimental and parametric analysis

This mixture contains dense particles with irregular shape whose particle size averages between 40-50 µm.[10] Thermal spraying plays a significant role in the technologies employed for surface modification is

capable of imparting thick coatings over ~100-120 µm over a large area in shorter time in comparison with conventional coating processes namely the electroplating, CVD and PVD.[11] AISI 1020 acts as a universal material owing to its cost effectiveness, simplicity in fabrication and for exhibiting good corrosion resistance. Nickel stabilizes its austenitic phase. Nevertheless, austenitic phases show higher possibility for localized attack in applications due for longer spans and reveal intense biological effects. Corrosive products comprise of chromium, iron, and molybdenum and nickel etc. Accumulated ions in tissues around the implant are carried to various parts of the body. The reports illustrate that the resulting metallic ions from austenitic steel's vitro corrosion cause undesired alterations.[12] As reported in literatures, bond coating posses' severe functionality issues which is attributed to differential thermal expansion coefficient prevailing between the substrate and coating materials.[13] In case of substrate and Al_2O_3 and TiO_2 coating mixture, it is imperative to ensure match of thermal expansion between coating and substrate layers. Nevertheless, it has to be ensured that bond coatings are typically thinner than main coatings.[14,15] Further, the implications on including carbon nano tubes in feed powders have not been reported in detail which demands an intensive study owing to the favourable features it would impart to the coating materials due to its favourable mechanical and chemical properties.

The idea behind this investigation is to determine the influence on mechanical properties and metallurgical behaviour due to Al_2O_3–13 wt% TiO_2 with 1% carbon nanotube (CNT) mixture of coating material layered on AISI 1020. Subsequently, the quoted specimens are characterized by XRD, SEM etc. ASTM C-633 standards are used for bond strength evaluation. RSM is employed for examining the parametric effects. The work scheme to be followed is briefly presented in the flowchart in Fig.-2.

EXPERIMENITAL

Materials and Methods

The plasma spray technique shown (Fig.-3) consists of power supply, DC plasma spray torch, gas feeding system, control console, powder feeder and water cooling arrangement.

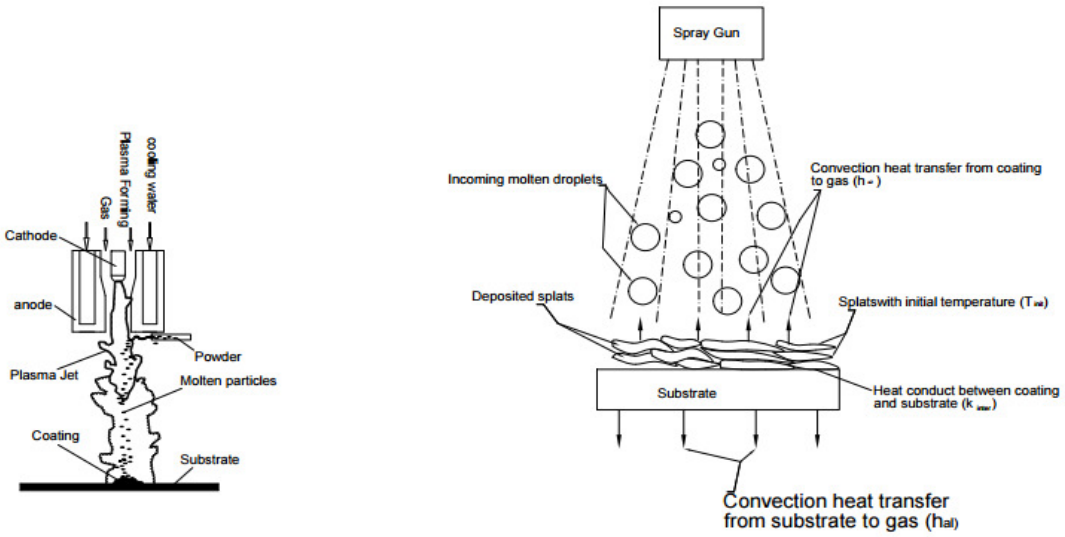

Fig.-3: Plasma spray mechanism[16]

Plasma torches functions in non-transferred mode with gas flow rates high and currents respectively. The energy from the arc is extort by plasma, while pushing out of torch nozzle with a velocity as high as 600-800 m/s and temperature of as high as (10,000-20,000K). Ceramic or Metallic powder are introduced into plasma jet gets melted and the droplets hits the surface of the substrate with towering velocity thereby creating an adherent coating. The dc plasma spray equipment and its basic working is illustrated (Fig.- 4). Tungsten rod forms the cathode tip of conical shape. Nearly 2-3% thorium oxide is supplemented to

tungsten to enhance its thermionic emission. Copper is used for the nozzle and nylon blocks insulated acts as a separator between the electrodes.

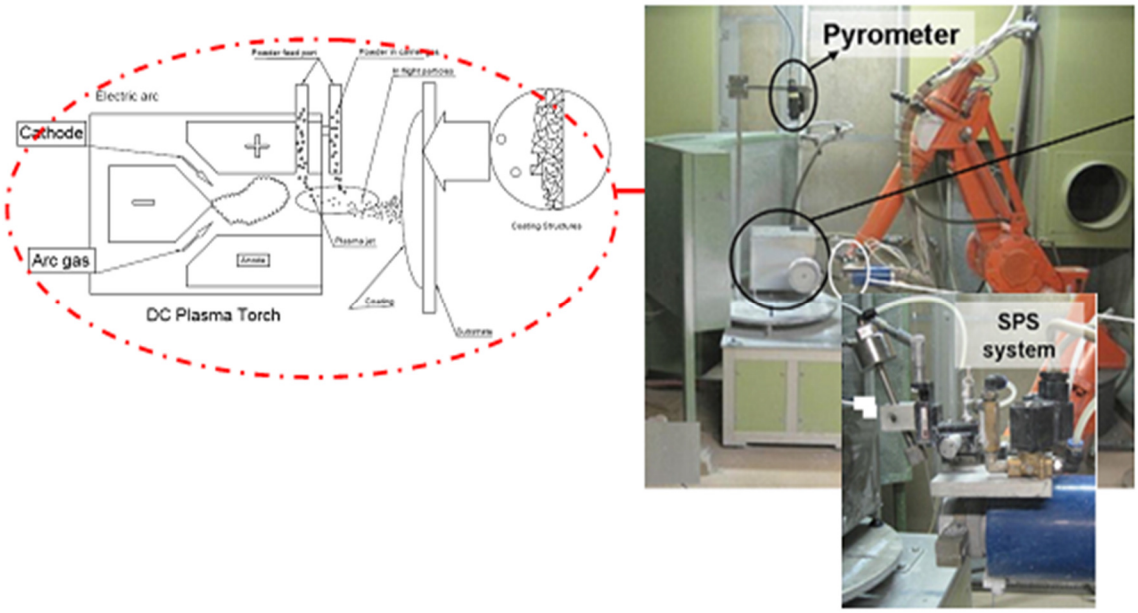

Fig.-4: Plasma Spray Equipment

Argon as plasma is injected into the inter region of electrode along the side port within insulator. Water cooling is used for the electrodes and the nozzle is fixed with a port close to its edge that enables the carrying of powders and feeding gas. Upon the striking of electric arc between the electrodes, energy from the arc is extracted by the plasma that rushes out of the nozzle with high temperature and velocity jet respectively. The combined action produces a thermal pinch effect at the cold wall and nozzle and forms a cold sheath of gas along the arc column which is highly conductive and exhibits a very high temperature. Coating powders introduced into the stream of plasma jet melts the particles that travel at velocity as high as 100 m/s directed onto the substrate surface and subsequently solidify into an adherent coating. The nozzle dimensions used are diameter 6 mm, gap between electrodes maintained at 12 mm and length of cathode 50 mm. The operational parameter setting which is maintained constant is provided in Table-1.

Table 1: Operational Parameter

Parameters	Range
Operating Power	1-21KW
Current	500A
Voltage	65V
Flow rate of plasma gas (Ar)	80LPM
Flow rate of secondary gas (H_2)	15LPM
Spray Distance	2.5”
Coating thickness	250Micron

Several trials are carried out by varying the experiments based on design of experiments and Table-2 presents the details of the combination of parameter values for each trial.

Table-2: Experimental parametric levels (minimum and maximum values) of the variable

Variable spray process parameter	Description	Min Level	Central Point	Max Level
X1	Plasma Power (kW)	20	30	40
X2	Feed rate (g/min)	6	14	22

X3	Scanning speed (mm/s)	200	350	500
X4	Number of cycles	10	15	20

Coated Sample

The plasma sprayed surface modified specimens with varying clad layer compositions viz., AL_2O_3:13%TIO_2: CNT is shown in Figure-5.

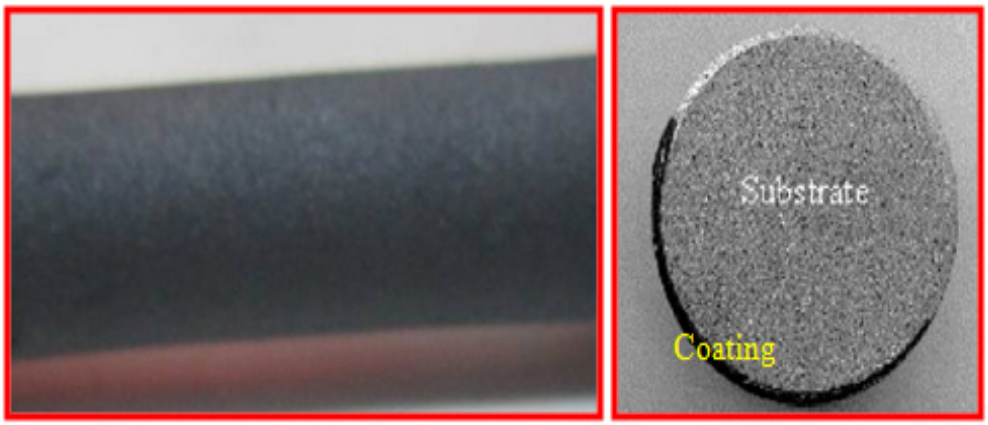

Fig.-5: Al_2O_3:13%TIO_2: CNT

Response Surface Methodology for parametric analysis

Experimental investigations are made to access the strength aspects of the coatings followed by RSM for parametric analysis. RSM combines tools of mathematics and statistics for model building, simulation and analysis of intricate problems wherein the response of interest is affected by innumerable variables and optimization of the response being framed as the key objective[16], the universal model equations in RSM used for the study is as follows:

$$y = \varepsilon_0 + \sum_{i=1}^{b} \varepsilon_i x_i + \sum_{i=1}^{b} \sum_{j=i+1}^{b} \varepsilon_{ij} x_i x_j + \sum_{i=1}^{b} \varepsilon_{ii} x_i^2 \quad (1)$$

Where, y is the response while the power of plasma, scanning speed, rate of feed and number of cycles forms the inputs and $\varepsilon 0$, ε i , ε ij and ε ii indicates the constant, linear, quadratic and interaction terms respectively.

Modelling of the process with RSM that incorporates statistical DOE accounting for the design of central composite face centred is a reliable tool.[17] They provide key information's on the interaction and main effects while reducing the time consumed and costs incurred. For this investigation, response surface (RS) model of 2nd order for forecasting the strength Alumina, TiO_2, CNT powder coated samples strength. Engineering associated industries find it essential to determine regions an improvement response is observed apart from optimum response.[18] RSM models accuracy is validated generally in terms of the results obtained from experiments. Here, the RSM model is used for determining the plasma coatings optimum conditions that would yield maximum strength. Taguchi's method has been commonly employed for process parameters optimization. The error percentage among the predicted values and experimental results was negligible. Mechanical property variations are also addressed with the coated samples microstructures.

RESULTS AND DISCUSSION

RSM results

ANOVA technique[19] is used to verify the developed models adequacy at a confidence interval 95%. The table comprises of sum of squares attained from the 1st order terms while the lack of fit, experimental error and the 2nd order equation contributing to the degrees of freedom. In accordance with ANOVA

technique, the adequacy of the model is obtained within the confidence level, if the value of the *F* ratio calculated show lack of fit while the original error limits to the standard *F*-ratio tabulated.[18-19] Here power of plasma, speed of scanning, rate of feed and number of cycles is sufficient and exist in non-linear form as shown in Table-3.

Table-3: Analysis of Variance (ANOVA) for Alumina, TiO_2 and CNT coatings

X1 (Plasma Power kW)	X2 (Feed Rate g/min)	X3 (Scanning Speed mm/s)	X4 (Number of cycles)	Y1 Micro hardness (HV)	Y2 Thickness/Cycle (µm)	Y3 Deposition Efficiency	Y4 Porosity (%)
40	22	200	10	878	31.24	76	2.90
40	6	500	10	798	75.5	46	4.44
20	22	500	10	719	63	42	6.58
20	6	200	10	622	15.61	34	11.56
20	6	500	10	687	49.72	30	5.88
20	6	500	20	663	17.92	26	6.02
40	6	500	20	778	35.26	51	4.86
40	22	200	20	831	21.32	69	2.74
40	22	500	10	782	79.86	56	3.53
20	22	200	10	692	24.56	57	3.77
20	22	200	20	695	9.94	56	5.36
20	6	200	20	615	13.44	68	5.92
40	6	200	20	831	12.16	70	4.16
40	22	500	20	778	35.61	46	4.82
20	22	500	20	648	29.22	32	5.80
40	6	200	10	843	27.84	50	4.80
30	14	350	15	864	42.88	62	4.98
30	14	350	15	850	37.47	53	3.72

Tests are imperative to determine the regression models significance that involves individual model coefficients and test for lack-of-fit test for significance. ANOVA table facilitates the experimental tests performed. Table-3 depicts ANOVA outcome model for response surface recording the adopted levels for the different parameters. The F value is less than 0.05 for the model indicating the significance of the model. It is clearly evident that the model terms have considerable impacts on the response. On similar lines, the main effect of feed rate (X2) and plasma power (X1) are the interaction at two levels that dictates the significant terms of the model. The contribution of the model terms is negligible. Other model terms that are insignificant (un-accounting those essential to support hierarchy) may be get rid of to evolve an improved model. Lack-of-fit also shows insignificant. Such models are essential to accomplish proper fit. The power of plasma and rate of feeds main effect is highly significant factor governing the specimen coatings. Results yield variability measure in the observed values of response and is illustrated by controllable factors along with their interactions. The completed mathematical models typically in coded forms is employed to forecast the optimal or the best coating conditions of alumina, TiO_2 and CNT blends to attain optimal thickness, hardness, efficiency of deposition and porosity as given below:

Regression Analysis: Y1 versus X1, X2, X3, X4

Regression Equations:

$$Y1 = 569.5 + 7.36\ X1 + 1.45\ X2 - 0.0642\ X3 - 2.28\ X4 \quad (2)$$

$$Y2 = 14.1 + 0.596\ X1 + 0.370\ X2 + 0.0958\ X3 - 2.406\ X4 \quad (3)$$

$$Y3 = 39.5 + 0.744\ X1 + 0.461\ X2 - 0.0629\ X3 + 0.337\ X4 \quad (4)$$

$$Y4 = 10.53 - 0.1165\ X1 - 0.0948\ X2 + 0.00030\ X3 - 0.0473\ X4 \quad (5)$$

Equations-2 to 5 present the regression equations depicting the extent of input parametric dependencies on out parameter. The main effects plot allows researchers to arrive at clarity on the main effects of parameters that are interdependent in the process. Main effect is typically estimated by deducting the overall mean (for the factor) from the mean of each level. The Figure 6-13 indicates the main effects location for the various input parameters and the coating strength respectively. Therefore, the feed rate, plasma power, scanning speed tends to increase while moving along low to high level respectively. Consequently, each level of the factors alters the response in a different way. At high level of each factor mean responses are obtained and subsequently compared to responses at low level. Besides, the plasma power seems to illustrate greater effect on the responses when compared with the attained slope.

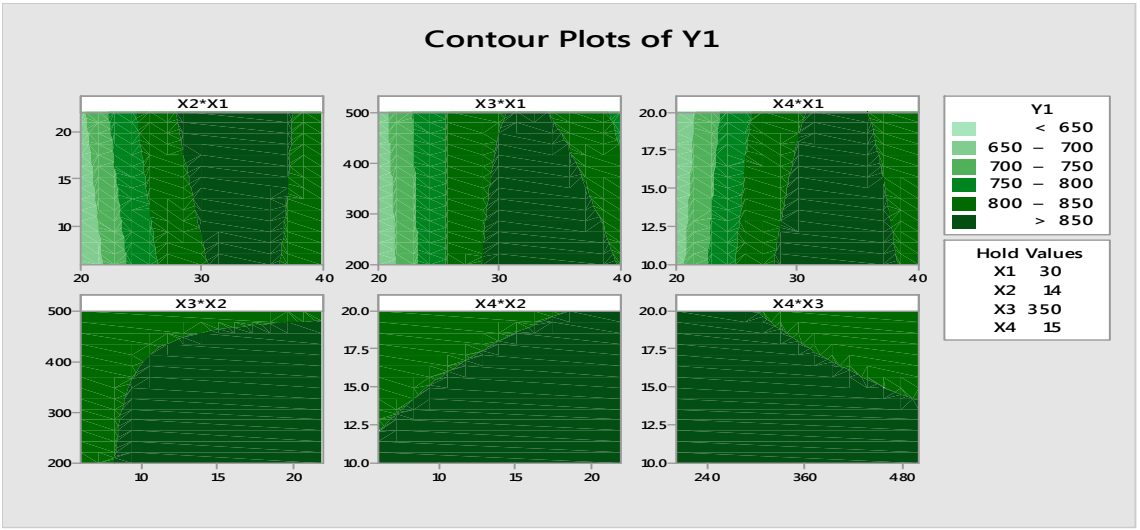

Fig.-6: Contour plot for plasma power Vs various input parameters

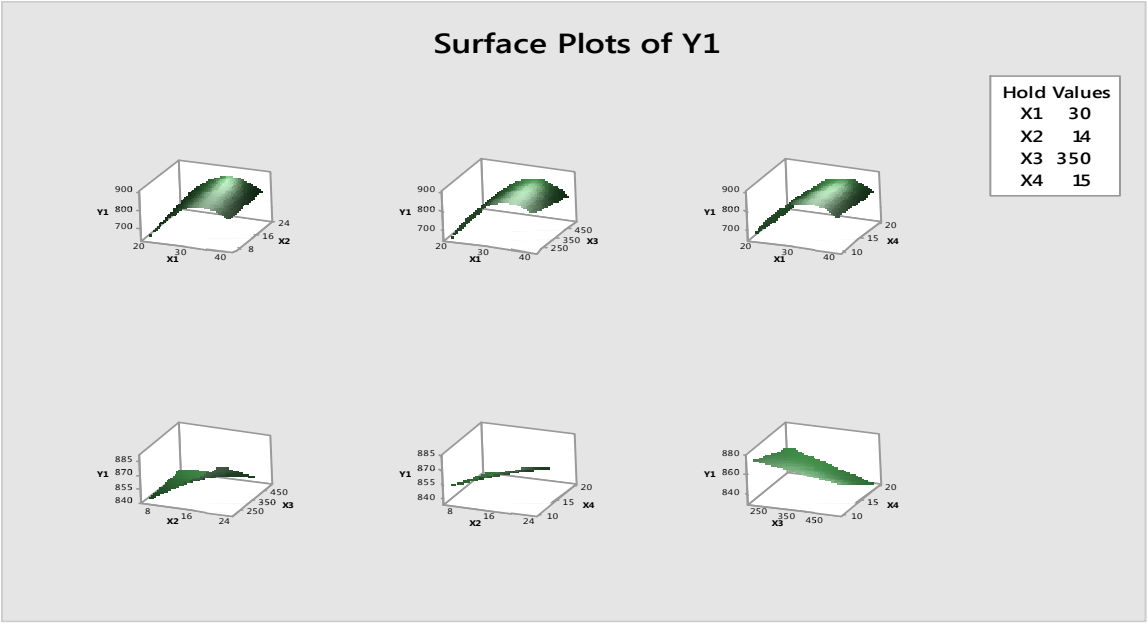

Fig.-7: Surface plot for plasma power Vs various input parameters

Accomplishing the response surface's shape; valleys, hills, and ridge lines are done through surface plot. Therefore, the Equations- 2 to 5, function *f* (*X1, X2*) can be plotted versus the *X1* and *X2 levels* (Fig.-7). From the plot, it's observed that each individual value of *X1* and *X2* produce a *y*-value. This 3D graph

illustrates the response surface. The contour plots Figs.- 6 to 13 are produced using Eq.2-5, the estimated fit coefficient is achieved by maintaining any one variable constant as "hold values" (Figs.- 6 to 13).

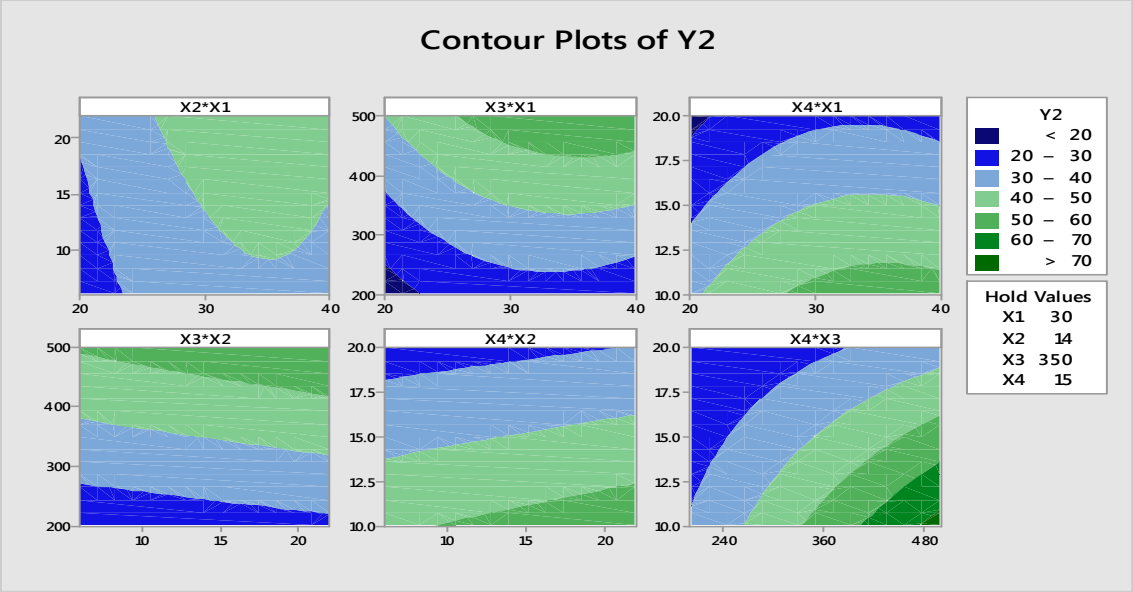

Fig.-8: Contour plot for feed rate Vs various input parameters

Contour plot suggests prominent alterations in the strength of the coating resulting from feed rate and plasma power which is evident from the increasing strength of coating while moving along the axis depicting the plasma power and axis depicting the feed rate. ANOVA results acknowledge that the plasma power is significant while feed rate shows contradicting response. The curve representing the coating strength at varying feed rate and varying ranges of plasma power are easy to understand. Besides, the coating strength slope in terms of plasma power indicates negligible change in feed rate.

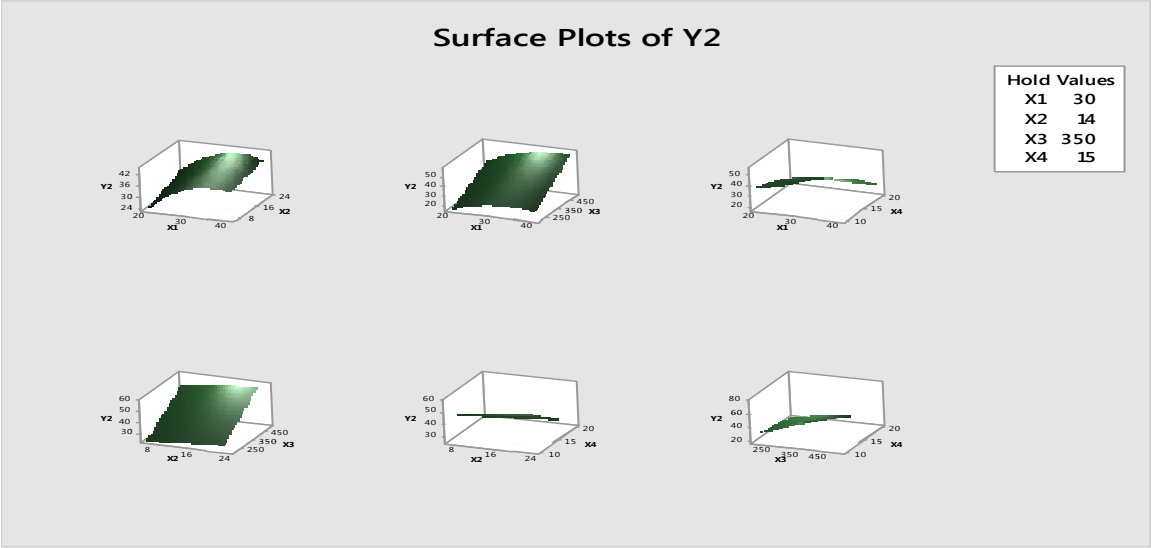

Fig.-9: Surface plot for plasma power Vs various input parameters

Micro-structural study of the coatings for surface morphology

Inter bonding among particles of powders sprayed and the coating morphology dictates the interface adhesion between the substrate and the coating layer. The micro-structural images of the substrate coated

with Al_2O_3: $13TiO_2$: CNT are shown in Fig.-14. The image exhibits a uniform distribution of the coat layer with semi-molten and molten particle undergoing agglomeration to form laths. Some negligible amount of cavitations is also observed. Few pores are noticed on inter and intra particle circumferences, boundaries and triple particle at grain junctions.

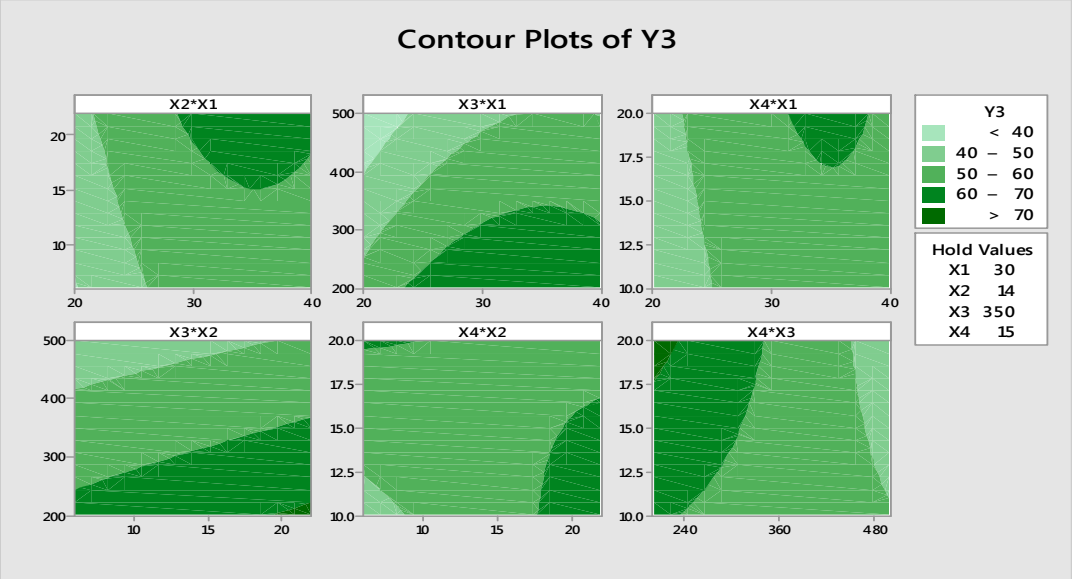

Fig.-10: Contour plot for Scanning Speed Vs various input parameters

This may be attributed to the fact that in those areas exhibiting pores, there may be insufficient molten particles flow during solidification. The deposition of coating is carried out at 15kW that indicates a smooth but different morphology i.e. spheroid splats are clearly observed, that indicates absolute particles melting in the process of plasma's in-flight traverse through jet of. Negligible number of cavitations is noticeable within the boundaries of the inter-granules. Particles receive more thermal energy in the process of solidification from molten state. This leads to the agglomeration forming splats i.e. flattened region is created. Subsequently, a negligible number of cavitations is recorded which improved adhesion at the interface of the coating on substrate thereby enhancing their adhesion strength.

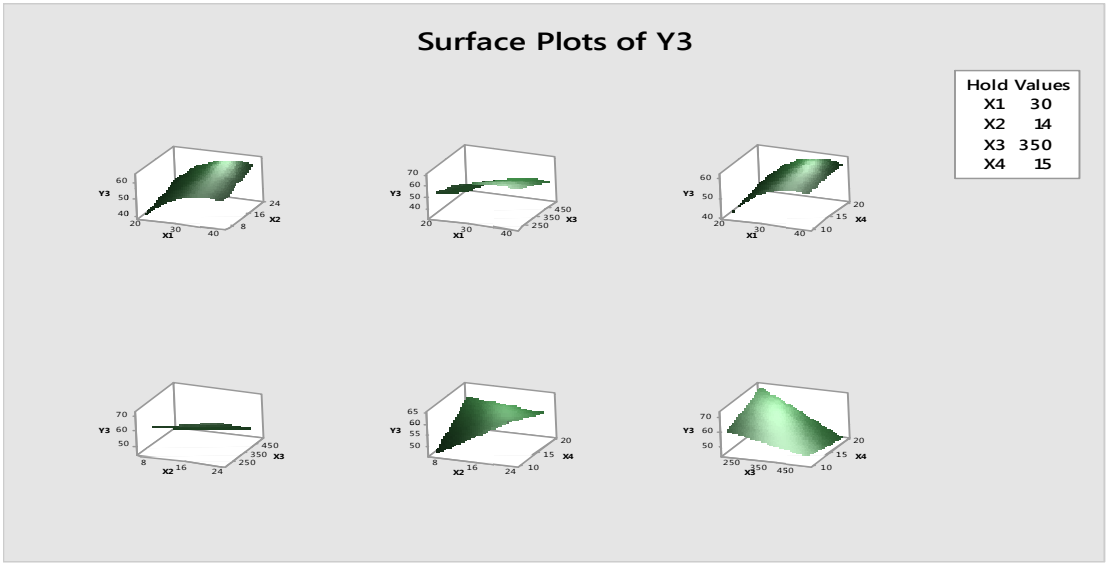

Fig.-11: Surface plot for plasma power Vs various input parameters

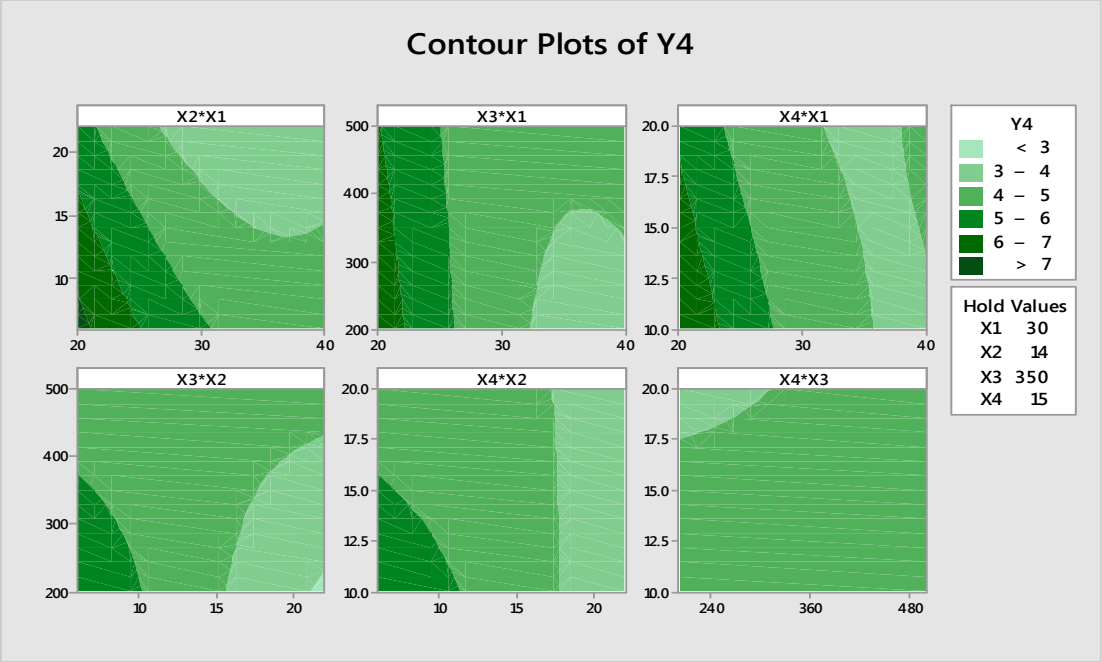

Fig.-12: Contour plot for Number of Cycles Vs various input parameters

Hardness and XRD

The coated layer's hardness is measured by Vickers micro-hardness equipment and the values are presented in table 2. The samples before getting subjected to loading, is polished and the cross sections are subjected to a load of 100 g. Indentation basic parameters are set to 10 s. The thickness of the coatings on an average is arrived based on 10 measurements. Post the deposition process; samples gluing to pull rods are performed to estimate the strength of bonded coatings which are measured by universal testing machine with cross head speed of about 0.5mm/ min. 5 samples are tested from each group used in each group.[20] Rigaku-type diffractometer with a Cu Ka radiation is used to obtain XRD plots which operate at a wavelength of 1.54056A˚ to examine the phase changes in the coatings.

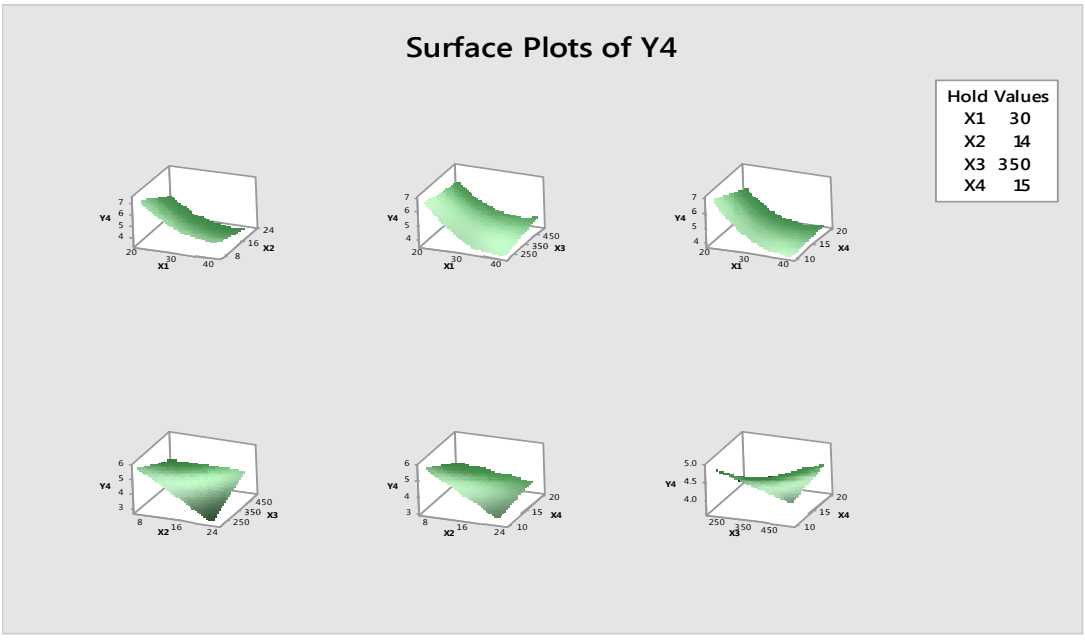

Fig.-13: Contour plot for Number of Cycles Vs various input parameters

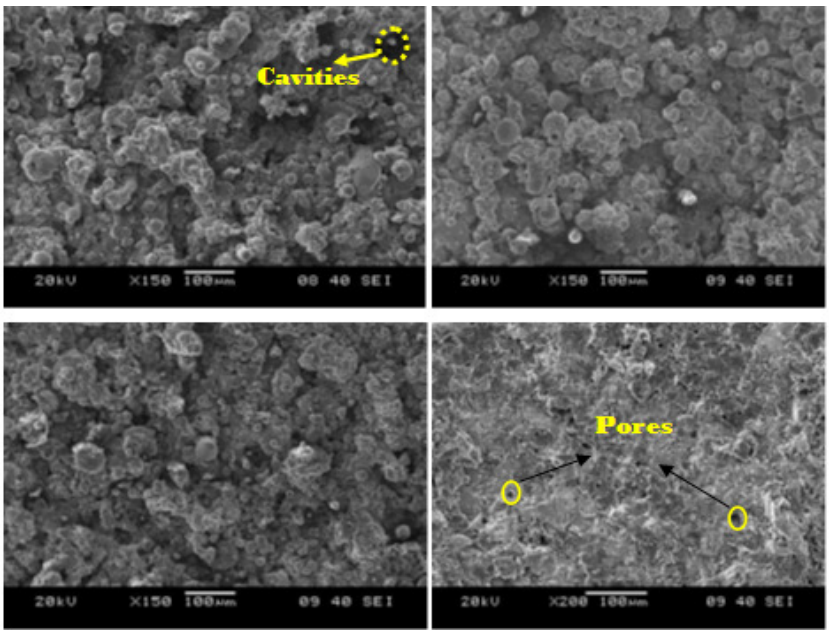

Fig.-14: Micro-structural images of Al_2O_3: 13TiO_2: CNT coating on substrate

From the Figure-15 Al_2O_3 phase formation is prominent (Fig.-15). Studies using XRD illustrate the presence of the dominant compound in coated layer post the formation of g-Al_2O_3 including some a-Al_2O_3 and iron oxides. Studies recorded by Goberman[10] also illustrated that higher CPSP supports the formation of g-Al_2O_3. This observation implies a good coherence between the experimentally recorded results and the once reported in the literature. Al_2O_3 in the conventional coating techniques are attributed to both unmelted feed particles and solid-state g-to-a phase transformation.[10] However, there are no traces of new inter-metallics or impurities which may ruin the quality of the coating.

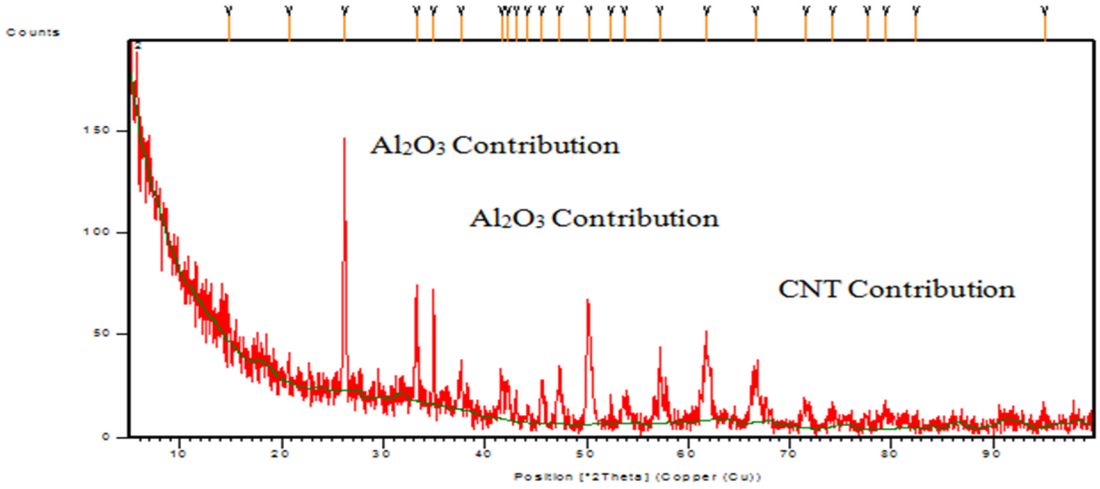

Fig.-15: XRD result of Al_2O_3, TiO_2 and Carbon nanotube sprayed on AISI1020

SEM with EDAX

Plasma sprayed coated specimens are investigated using SEM to understand the morphology at the interface of the coatings (Fig.-16). Key objective of obtaining SEM images is to ascertain spheroidisation phenomena during the agglomeration process of particles. The coated samples are polished with abrasive papers made of SiC along the cross section with varying grit sizes in three stages. The samples with

dimensions of 20 mm x 5 mm rectangular size are sliced from the original coated specimens and are mounted with the aid of moulding powders of thermosetting nature.

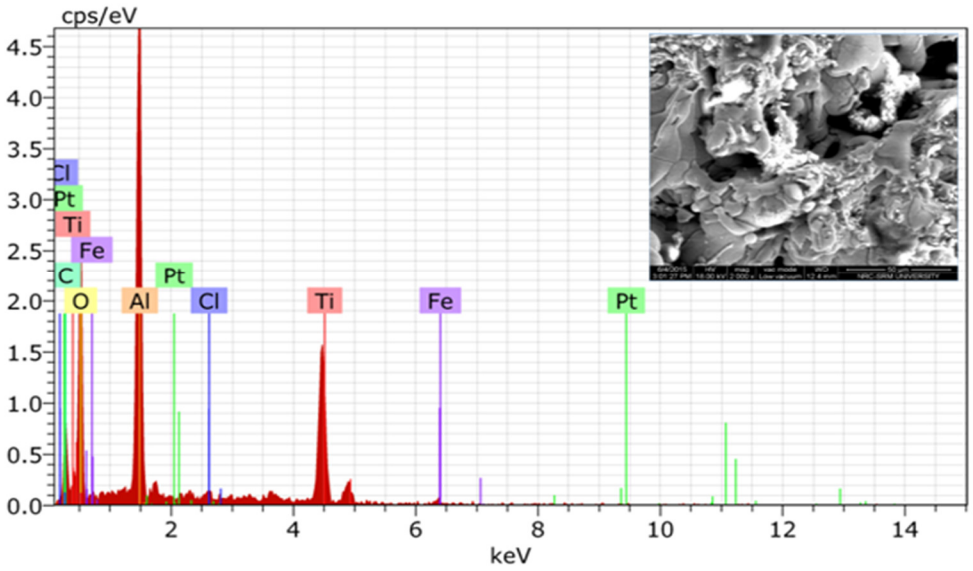

Fig.-16: SEM with EDAX for Alumina + 13TiO_2+CNT

The particles are irregular in shape as observed from Fig.-16 due to difference in their rate of solidification. Particles are of elongated and versatile in nature. The particle size analysis shown in Fig.-16 is estimated to be 61.78 µm from calculations. The morphology of alumina plasma sprayed powder processed at 15 kW power and collected at 100mm standoff distance (Figure-16). Most of the particles are spherical in shape. Some particles, of larger diameter have been cracked, may be due to thermal pinch effect/fragmentation. At some places coagulation of particles is also observed in the figure; along with some unmelted powder particles. When the standoff distance increased to 400mm, it exhibits a different morphology as shown in Fig.-16.When the alumina ball milled powder, after being plasma processed at 15kW power, is collected at 100mm and 400mm standoff distances, there is a drastic change in particle shape and size as observed in the SEM image. All the particles have achieved solidification state following the complete molten state.

CONCLUSION

Steel is surface modified by adding CNT along with TiO_2 and Alumina coating mixture respectively using plasma spray technique forming a composite at its surface. Scanning electron microscopy results confirms the presence of CNT's in the matrix of the steel. Subsequently, crystalline size of the sharp peak of iron is reduced remarkably and an average grain size is reduced from micrometers to nanometres. Besides there is a prominent reduction in the stress and strain estimated at around 3 times as compared to the samples received. The measured lattice constant after the reinforcement of CNT's is in the order equal to the standard data. The hardness of steel increased to about 30% after the reinforcement of CNT's. Hence, plasma spray technique is observed to be an effective mechanism to change the mechanical properties of steel owing to its effectual localized heating capability. As steel finds greater industrial applications, plasma spray technique establishes its feasibility to enhance microstructure and mechanical properties at optimized cost. Added to this, CNT's create a material revolution as it yields a remarkable feature in terms of surface modification. Response surface methodology reveals that plasma power and the rate of feed are the key parameters governing the quality of the coating.

REFERENCES

1. G. Lallemand–Tallaron, Ph. D Thesis, EC Lyon, France, (1996).
2. S. Das, Ph. D. Thesis, NIT Surtakal, India, (2007).

3. K. Katiki, S. Yadlapati, S.N.S. Chidepudi, M. Manikandan, M. Arivarasu, K. Devendranath Ramkumar and N. Arivazhagan, *Int. J. ChemTech Res.*, **6(5)**, 2744 (2014).
4. B. Venkateshwarlu, M. Mohan Jagadeesh Kumar, *Int. J. ChemTech Res.*, **8(1)**, 141 (2015).
5. HJ. Grabke, G. Kurbatov, HJ. Schmutzler, *Oxid. Met.*, **43(1)**, 97 (1995).
6. JL. Smialek, BK. Tubbs, *Metall. Mater. Trans. A.*, **26(2)**, 427 (1995).
7. Lech Pawlowski, The Science and Engineering of Thermal Spray Coatings, John Wiley & Sons, New York, 218(1995).
8. S.C. Mishra, 2012, Analysis of Experimental Results of Plasma Spray Coatings Using Statistical Techniques, Advanced Plasma Spray Applications, InTech, pp. 83-96.
9. GK. Beshish, CW. Florey, FJ. Worzala, WJ. Lenling, *J. Therm. Spray Tech.*, **2(1)**, 35 (1993).
10. T.J. Steeper, A.J. Rotolico, J.E, Nerz, In Proceedings of National Thermal Spray Conference for Optimizing plasma sprayed alumina-titania coatings using statistical methods, Anaheim, CA, pp. 7–11 (1993)
11. J.D. Majumdar, *Surf. Coat. Technol.,* **205(7)**, 1820 (2010).
12. S.P. Sharma, and S.C. Lakkad, *Composites Part A*, **42(1)**, 8 (2011).
13. F. Inam, D.W.Y. Wong, M. Kuwata, and T. Peijs, *J. of Nano Mater.*, **9**, 1 (2010).
14. Ajit Behera and S.C. Mishra, *J. of Mater. & Metall. Engg.,* **2(1)**, 23 (2012).
15. Harminder Singh, T.S. Sidhu, S.B.S. Kalsi and J. Karthikeyan, *J. Braz. Soc. Mech. Sci. & Eng.*, **35(3)**, 231 (2013).
16. Montgomery, C. Douglas, Design and Analysis of Experiments: Response surface method and designs, John Wiley and Sons Inc, New Jersey pp. 21, 201(2011).
17. Myers, H. Raymond, Andre I. Khuri, and Walter H Carter, *Response Surface Methodology, Technometrics,* **31(2)**, 137 (1989).
18. V.N. Gaitonde, *J. Mater. Process. Technol.,* **195**, 225 (2008).
19. Nuran Bradley, Master of Science Thesis, The Response Surface Methodology, Indiana University South Bend, (2007).
20. Gurusami, K., K. Shanmuga Sundaram, N. S. Azhagarasan, and R. Vijay, *J. Balk. Tribol. Assoc.,* **21(4)**, 866 (2015).

[RJC-1707/2017]